

ALMA Memo 321

Receiver amplitude calibration for ALMA

Richard L. Plambeck
Radio Astronomy laboratory, University of California, Berkeley, CA 94720

August 27, 2000

Abstract

I consider the problem of calibrating the amplitude scale for the ALMA receivers, focussing particularly on the question of whether cold loads are necessary to achieve the best possible accuracy. Cold loads are of possible value below about 300 GHz. In these lower frequency bands the atmospheric opacities are low, so the sky appears cold; and SIS mixers are more likely to exhibit gain compression, so it is best to calibrate them with loads which are similar to the sky temperature. I estimate, however, that reflections and losses in dewar windows will likely lead to calibration uncertainties of at least 3% with cold loads, and argue that they are not worth the complexity.

Calibration techniques where the loads intercept only a fraction of the receiver beam can achieve better accuracy. One possibility is to mount the loads behind a hole in the center of the subreflector, as described by Bock et al. in ALMA memo 225. Another possibility, a variant of the traditional chopper wheel method, is to block the beam with a partially transparent vane. An advantage of the latter method is that the load filling factor, or absorption of the vane, may be calibrated on the telescope with an astronomical observation; furthermore, this technique may be useful for calibrating solar observations.

Measuring the atmospheric opacity with a specialized instrument at the center of the array may be preferable to calibrating it separately at each antenna. I estimate that the opacity varies by $\sim 3\%$ over scales of 1.5 km.

1 Introduction

The ALMA Scientific Advisory Committee has set a target of 1% for the absolute flux calibration accuracy of the instrument. How should the receivers be calibrated in order to achieve (or at least, to approach) this goal? What hardware is required?

Several previous ALMA memos consider these questions. Yun et al. (1998, memo 211) argue that the standard chopper wheel calibration gives no better than 5% accuracy, and advocate a method where calibration signals are coupled to the receiver through a hole in

the center of the subreflector – a technique described in more detail by Bock et al. (1998, memo 225). Mangum (2000, memo 318) provides a detailed mathematical description of the calibration process; he presents estimates of the calibration uncertainty at 230, 490, and 650 GHz which suggest that the subreflector calibration technique can approach the target of 1% absolute accuracy.

Because the subreflector calibration method has not been thoroughly tested, and because some of the assumptions in the previous memos may be overly optimistic, the receiver design group has been hesitant to rule out other calibration options – in particular, the use of cold loads. To help guide these decisions, this memo provides estimates of the amplitude calibration accuracy obtainable with the following techniques:

1. Conventional “chopper wheel” calibration with a single 290 K load.
2. Modified “chopper wheel” calibration with a semitransparent 290 K load.
3. Calibration with two loads which fill the receiver beam. Three possible temperature combinations are considered: 290 K and 350 K; 290 K and 80 K; and 80 K and 20 K.
4. Calibration with 300 K and 400 K loads mounted in the subreflector, subtending 0.8% of the receiver beam.

The sources of uncertainty considered are:

- Imperfect knowledge of the atmospheric temperature and opacity.
- Uncertainty in the effective temperatures of the loads.
- Imperfect knowledge of the receiver sideband response.
- Uncertainty in the spillover efficiency and effective spillover temperature.
- Gain compression in the SIS mixer or following amplifiers.

Two sources of uncertainty not considered are thermal noise, which generally is inconsequential for the GHz-wide bandwidths considered for ALMA; and receiver gain drifts, which are expected to be of order 10^{-3} or less over the time span between calibrations. Also, I ignore the effects of pointing errors, antenna gain variations, and decorrelation from atmospheric or instrumental phase noise, any of which could dominate the calibration uncertainty at higher frequencies.

I focus on the problem of calibrating the gain of a single receiver; for interferometric measurements made with a cross-correlator, the gains and system temperatures should be the geometrical means of those on individual antennas.

2 Methodology

Given the observing frequency, atmospheric opacity, and so on, I compute the output power from the receiver when it looks at the sky, at the source (a spectral line in one sideband of the receiver), and at the load(s). From these simulated observations, I work backwards to derive the source antenna temperature, while making incorrect assumptions about each input parameter in turn to determine what error this introduces. The receiver output powers are given by:

$$\begin{aligned}
 P_{sky} &= K(T) \{ T_{sky} + T_{rcvr} \} \\
 &= K(T) \{ G_s [\eta_l J(\nu_s, T_m) (1 - e^{-\tau_s A}) + \eta_l J(\nu_s, T_{bg}) e^{-\tau_s A} \\
 &\quad + (1 - \eta_l) J(\nu_s, T_{spill})] + G_i [\eta_l J(\nu_i, T_m) (1 - e^{-\tau_i A}) \\
 &\quad + \eta_l J(\nu_i, T_{bg}) e^{-\tau_i A} + (1 - \eta_l) J(\nu_i, T_{spill})] + T_{rcvr} \} \quad (1)
 \end{aligned}$$

$$P_{source} = K(T) \{ T_{sky} + T_{rcvr} + G_s \eta_l T_A e^{-\tau_s A} \} \quad (2)$$

$$P_{load} = K(T) \{ f [G_s J(\nu_s, T_{load}) + G_i J(\nu_i, T_{load})] + (1 - f) T_{sky} + T_{rcvr} \} \quad (3)$$

Here

$$J(T) = \frac{h\nu}{k} \frac{1}{e^{h\nu/kT} - 1} \quad (4)$$

is the equivalent Rayleigh-Jeans temperature of a black body with physical temperature T , and the other symbols are defined in Appendix A. These expressions are similar to those used by Ulich & Haas (1976) and Mangum (2000), with 2 key differences:

- The loads need not completely block off the sky, but instead are assumed to fill fraction f of the receiver beam. This allows for the case where the loads are mounted at the center of the subreflector; alternatively, f may be interpreted as the attenuation of a semitransparent vane which covers the entire beam.
- To model receiver gain compression, K is not assumed to be constant, but is a function of the effective input temperature T .

The simulated observations were for a source at 1.5 airmasses, at frequencies of 110, 230, and 490 GHz. The zenith opacity was taken to be 0.05 at 110 GHz, 0.07 at 230 GHz, and 1.1 at 490 GHz; DSB receiver temperatures of 20 K, 35 K, and 75 K were used. The computation of the source antenna temperature follows 1 of 2 paths:

2.1 1-load method

The conventional “chopper wheel” calibration requires measurements of only a single, ambient temperature load. The source antenna temperature is given by

$$T_A = \frac{P_{source} - P_{sky}}{P_{load} - P_{sky}} f \Delta T_{cal}, \quad (5)$$

where the factor f allows for the case of a semitransparent vane. ΔT_{cal} is given by equation (16) of Ulich & Haas (1976):

$$\begin{aligned} \Delta T_{cal} = & J(\nu_s, T_{spill}) - J(\nu_s, T_{bg}) + \frac{G_i}{G_s} [J(\nu_i, T_{spill}) - J(\nu_i, T_{bg})] \\ & + [e^{\tau_s A} - 1] \{ J(\nu_s, T_{spill}) - J(\nu_s, T_m) + \frac{G_i}{G_s} [J(\nu_i, T_{spill}) - J(\nu_i, T_m)] \} \\ & + \frac{G_i}{G_s} [e^{(\tau_s - \tau_i) A} - 1] [J(\nu_i, T_m) - J(\nu_i, T_{bg})] \\ & + \frac{e^{\tau_s A}}{\eta_l} \{ J(\nu_s, T_{load}) - J(\nu_s, T_{spill}) + \frac{G_i}{G_s} [J(\nu_i, T_{load}) - J(\nu_i, T_{spill})] \} \quad (6) \end{aligned}$$

With some rearrangement, this expression matches equation (20) in Mangum (2000).

It may seem surprising that the receiver gain can be derived from measurements of a single load. One should remember, however, that the sky observation is implicitly an observation of a second load – namely, the 2.7 K cosmic background radiation. It is useful to think of the chopper wheel calibration as a measurement of the receiver gain *outside* the earth’s atmosphere, as shown in Figure 1. If a large 290 K load could be towed into the receiver beam 100 km above the earth, one could compare the receiver output on this load and on the 2.7 K background to obtain a perfect calibration of the receiver gain, including all atmospheric losses. Because the 290 K load is mounted in the receiver cabin instead, one uses a model of the atmospheric and antenna losses to compute T_{cal} , the temperature of a fictitious load outside the atmosphere which gives the same receiver output. The corrections introduced by the model are small if the atmospheric opacity is low.

2.2 2-load method

A more obvious way of calibrating the receiver is to compute the gain from measurements of 2 loads, then solve for T_A :

$$K = \frac{(P_{load1} - P_{load2})/f}{G_s J(\nu_s, T_{load1}) + G_i J(\nu_i, T_{load1}) - G_s J(\nu_s, T_{load2}) - G_i J(\nu_i, T_{load2})} \quad (7)$$

$$T_A = \frac{P_{source} - P_{sky}}{K f G_s \eta_l e^{-\tau_s A}} \quad (8)$$

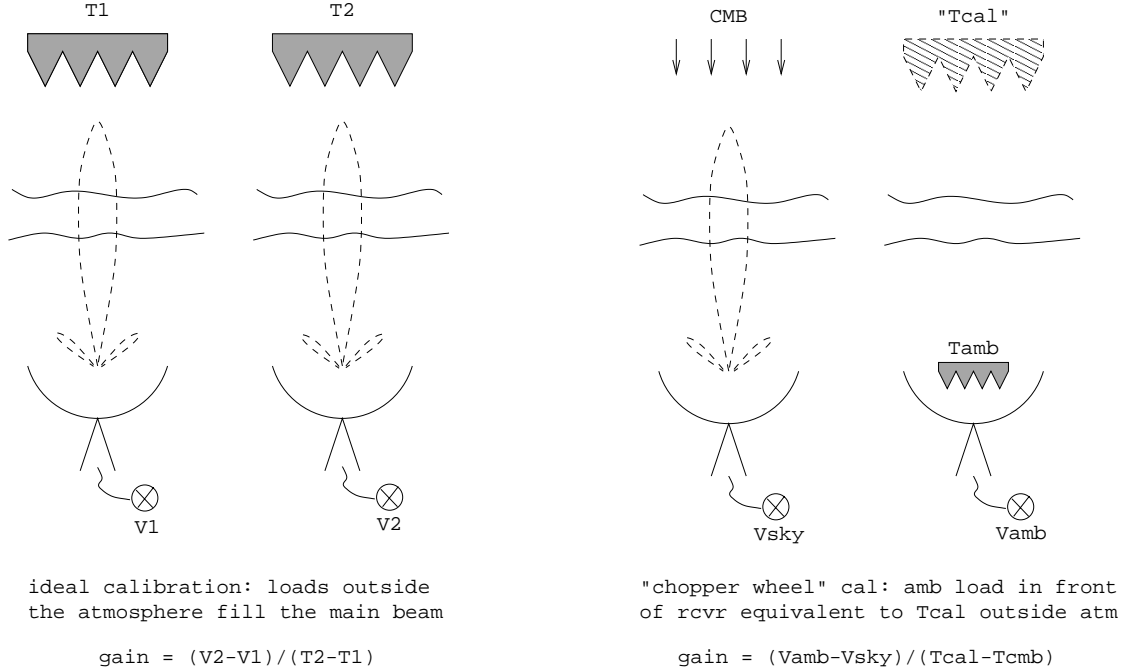


Figure 1: One may think of the chopper wheel calibration as a comparison between the 2.7 K background and a fictitious load at temperature $T_{cal} \sim T_{amb}$.

3 Justification of assumed uncertainties

3.1 Atmospheric temperature T_m

I assume that the mean atmospheric temperature T_m is known within ± 5 K. To obtain this accuracy it may be necessary to use radiosonde data or to probe the atmosphere with a 50 GHz radiometer which measures the brightness temperature of the optically thick oxygen lines. T_m appears explicitly only in the 1-load calibration formula; it may also enter indirectly into the measurement of τ , as discussed below.

3.2 Atmospheric opacity τ

I assume that τ will be measured with a specialized tipping radiometer or FTS spectrometer positioned at the center of the array. This instrument will make highly accurate measurements of the sky brightness temperature as a function of airmass. In the limit where $\tau \rightarrow 0$, these curves are straight lines with slope τT_m , and one must know the effective atmospheric temperature T_m to solve for τ ; this contributes an uncertainty $\Delta\tau/\tau \sim \Delta T_m/T_m \sim 2\%$,

if T_m is known to ± 5 K. At submm wavelengths $\tau \sim 1$, and it is feasible to measure the opacity from the curvature in a tipping curve – note, for example, that the change in the sky brightness temperature in going from 2 to 3 airmasses is $e^{-\tau}$ times the change in brightness from 1 to 2 airmasses. In the absence of detailed modeling or test observations, I assume that τ is uncertain by 2% in this case as well.

What about variations in τ across the array? At mm wavelengths both the atmospheric refractivity and absorption are proportional to the precipitable water vapor (PWV), so we can estimate the magnitude of the *opacity* fluctuations from the *phase* fluctuations measured with the 11.2 GHz site test interferometer. The median rms path fluctuation on a 300 m baseline at Chajnantor is 250 μm , according to the NRAO ALMA web page. These measurements are made at 36 degrees elevation and presumably should be divided by 1.3 to get the zenith value (Holdaway, et al. 1995). Since 1 mm of PWV introduces a path delay of about 6 mm, one infers that the rms fluctuations in PWV at zenith are of order 30 μm on a 300 m baseline. For a thin turbulent layer the fluctuations should scale as $d^{0.33}$, so $\Delta\text{PWV} \sim 50\mu\text{m}$ for $d = 1.5$ km. The median 225 GHz opacity, 0.06, corresponds to a total PWV of 1.5 mm, so $\Delta\tau/\tau \sim \Delta\text{PWV}/\text{PWV} = 0.033$ for antennas at the outer edge of a 3 km diameter array.

Combining the results above, I estimate that the total fractional uncertainty in τ is of order 4%. Could one do much better by measuring τ independently at each antenna? Possibly not – the water vapor fluctuations blow across the array at the wind speed, so the opacity over each antenna should vary by a few percent on time scales of minutes. Thus, periodically measuring τ at each antenna and applying this opacity correction to data taken over the next few minutes may be little better than continuously measuring τ at a central location and applying the time-averaged correction to all antennas. Of course, for the most extended antenna configurations it would be wise to monitor the opacity at a few additional locations in case there are large scale opacity gradients across the site.

A merit of the subreflector calibration technique is that it allows one to calibrate the sky brightness temperature continuously at each antenna, making it possible to follow rapid opacity variations. Alternatively, one could use the 183 GHz water vapor monitors to track these variations.

Here I do not consider the very important question of how accurately one can derive τ_s and τ_i , the atmospheric opacities in the signal and image sidebands, when these opacities differ. However, by measuring the sky brightness temperature over a wide range of frequencies with a special instrument at the center of the array, one can probably do a better job than by doing a tipping curve with each antenna just at the observing frequency.

3.3 Load temperatures

I assume that the effective physical temperature of each load is uncertain by 0.1 K, allowing for temperature gradients within the absorbing material and for errors in temperature

sensors. The load temperature need not be regulated to high accuracy, as long as it can be measured.

For loads which are not at room temperature, reflections from the absorber or windows in front of the absorber are likely to be the dominant source of error. The cold loads proposed for the ALMA receiver are inside the main dewar, and are viewed through dewar vacuum windows and infrared-blocking filters. Making the optimistic assumption that the power reflection coefficient from these components can be calibrated to 0.5% accuracy, and assuming that most of the reflected power is terminated at ambient temperature, I estimate that the effective load temperature is uncertain by

$$\Delta T_{\text{load}} = \sqrt{0.1^2 + [0.005(T_{\text{load}} - 290)]^2}. \quad (9)$$

Thus, the temperature of a 290 K load is uncertain by 0.1 K, while a 20 K load is uncertain by 1.35 K.

3.4 Load coupling factor f

The hole in the center of the ALMA subreflector is expected to intercept approximately 0.8% of the radiation from the feed horn (J. Payne, private communication). I will assume that this coupling factor is known to 1% – that is, the filling factor is 0.008 ± 0.00008 . Measuring the coupling factor to this kind of accuracy will not be easy. For comparison, preliminary measurements of the coupling to the loads in the prototype BIMA system vary by 10% with frequency, from 0.018 to 0.022, for unknown reasons.

In the case where the load is a semitransparent vane which intercepts the entire beam, f is interpreted as the absorption of the vane. The vane transmission can be calibrated on the telescope by making brief cross-correlation measurements of an astronomical point source, with and without the vane, then self-calibrating to derive the antenna-based gains for the 2 cases. For a 60-second integration, ALMA’s continuum sensitivity is predicted to be of order 0.1 mJy. The uncertainty in the amplitude gain for an individual antenna is greater by $\sim \sqrt{N}$, where $N = 64$ is the number of antennas. Thus, it should be straightforward to measure the gain to 1 part in 1000 on a 1 Jy source. The vane transmission is the ratio of two such measurements, so it is uncertain by 0.14%.

3.5 Mixer sideband response, G_s and G_i

Although many receiver bands will be outfitted with sideband separating mixers, these are likely to provide only 10–20 dB image rejection, so it will still be necessary to measure G_s and G_i . Probably this will also be done by making a short cross-correlation measurement of an astronomical point source. Signals in the upper and lower receiver sidebands can be separated in the correlator to high accuracy (to a few parts in 10^4 at BIMA) if the local oscillators on the antennas are phase switched by 90 degrees. By self-calibrating the

array separately on the signal and image sideband data, one can solve for G_s and G_i . The uncertainties will be dominated not by measurement errors, but by uncertainties in the spectral index of the source and in the atmospheric extinction corrections for the two sidebands, which differ in frequency by 16 GHz. If the flux density ratio of the 2 sidebands is known to 1%, G_i and G_s are uncertain by ± 0.005 .

3.6 Spillover efficiency η_l

I assume the spillover efficiency is uncertain by 0.5% and the spillover temperature is uncertain by 5 K.

3.7 Gain compression

It is because of receiver gain compression that we consider the possibility of providing cold calibration loads. If a perfect linear relationship existed between the input power to the receiver and the output voltage from a detector attached to the receiver, then loads at any temperatures would work equally well.

SIS mixers are likely to be the most important source of gain compression, although amplifiers and detectors could also contribute. For an SIS mixer voltage-biased at the peak of its gain curve, the gain can be approximated as (Feldman, Pan, & Kerr 1987)

$$K = \frac{K_0}{1 + (P_{sig}/P_{sat})} \quad (10)$$

For a series array of N junctions, mixer conversion loss L , and I.F. load impedance R ,

$$P_{sat} \propto \left(\frac{Nh\nu}{e} \right)^2 \frac{L}{2R} \quad (11)$$

(Tucker & Feldman 1985). For our purposes it is easier to specify a saturation *temperature* $T_{sat} \sim P_{sat}/(k\Delta\nu)$, where $\Delta\nu$ is the R.F. bandwidth downconverted to the I.F. Note that the saturation temperature scales as $(N\nu)^2$ – saturation is most likely to be a problem for single junction SIS mixers in the lower frequency bands.

What is a reasonable guess for T_{sat} ? Figures 2 and 3 show what I hope is a worst case example, based on measurements of a BIMA SIS mixer at 109 GHz. This is a single junction device which is well-matched over the entire 75–115 GHz band. The solid curve in Figure 3 shows that equation 10 fits the data very well; the saturation temperature is 315 K – that is, the mixer gain looking at room temperature load is about half the gain looking at a 20 K load. As shown by the dashed curve in Figure 3, biasing the junction on the side of the gain peak gives a nearly linear response – this is how the mixers are operated on the BIMA telescopes – at the expense of a slightly higher receiver noise temperature (in this case, 22 K DSB vs. 18 K DSB at the gain peak) and much greater sensitivity to

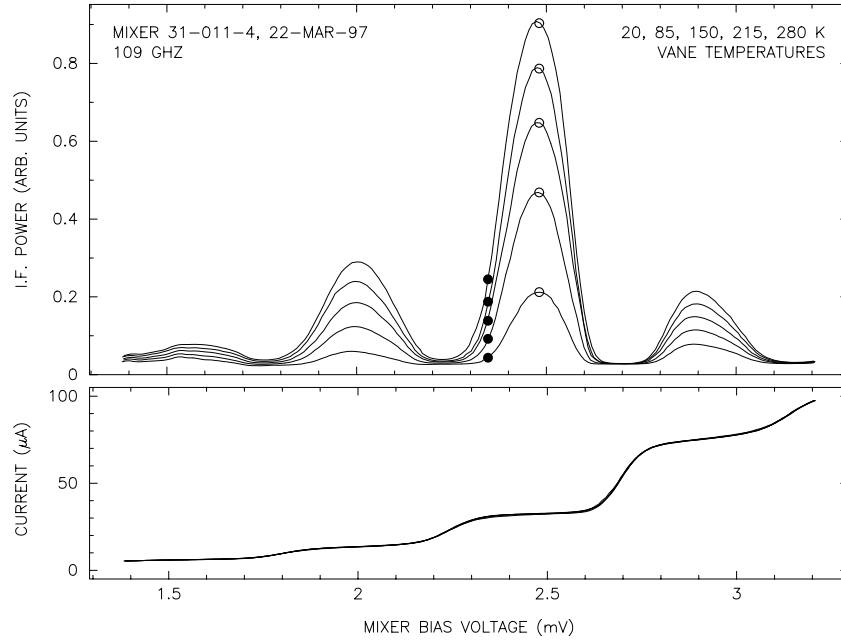


Figure 2: Tests of a BIMA SIS mixer, illustrating the effects of receiver gain compression. The top panel shows the receiver output power as a function of junction bias voltage for load temperatures of 20, 85, 150, 215, and 280 K. The bottom panel shows that the junction I-V curve was identical for all the tests. Adapted from Engargiola & Plambeck (1998).

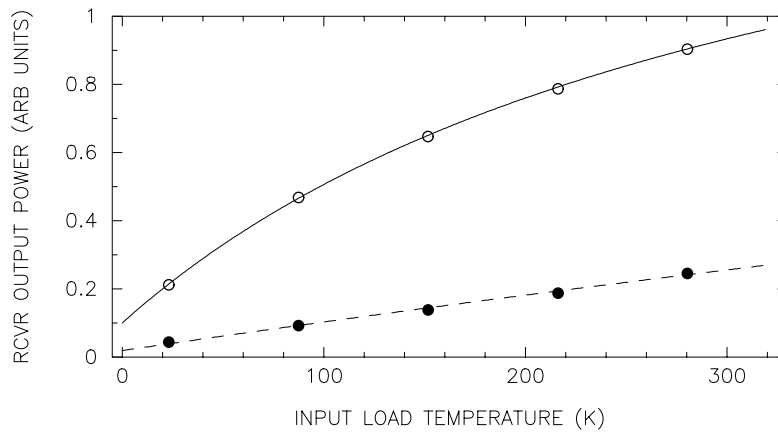


Figure 3: Fits to the I.F. power vs. input temperature using equation 10, for bias voltages of 2.48 mV and 2.35 mV.

temperature fluctuations (1% gain change for a 10 mK temperature change). The saturation temperatures are much higher for the two mixers tested by Feldman et al. (1987). At 114 GHz, a 2-junction SIS array gave $P_{sat} = 5.5$ nW, which corresponds to $T_{sat} \sim 10000$ K (assuming $\Delta\nu = 30$ GHz); while a 4-junction array gave $P_{sat} = 23.5$ nW, which corresponds to $T_{sat} \sim 40000$ K.

Because the saturation power is expected to scale as ν^2 , in the simulations I used $T_{sat} = 2500$ K at 110 GHz (10% gain compression on a 290 K load), $T_{sat} = 10000$ K at 230 GHz (3% gain compression on a 290 K load); and $T_{sat} = 50000$ K at 490 GHz (0.5% gain compression on a 290 K load). Hopefully these are pessimistic estimates.

4 Discussion

The fractional calibration errors computed from the simulations are summarized in Tables 1–3. One may draw the following general conclusions:

- Gain compression dominates the uncertainties at 110 and 230 GHz. It is of little concern at 490 GHz, partly because the SIS mixer saturation power scales as ν^2 , partly because the sky brightness temperature at 490 GHz is not all that different from a 290 K load.
- The atmospheric opacities are so low at 110 and 230 GHz that uncertainties in T_m and τ are not very important. If receiver gain compression were not a problem, the standard chopper wheel method would work beautifully at these frequencies. At 490 GHz, on the other hand, the calibration accuracy is determined almost entirely by uncertainties in T_m and τ .
- The assumption that the sideband gains G_i and G_s are uncertain by 0.5% contributes 1% calibration uncertainty to all methods. For observations of a continuum source, this error would be much smaller.

The following sections discuss the merits of the different calibration techniques.

4.1 Standard chopper wheel method

The standard chopper wheel method has the advantage of simplicity – it requires just a room temperature load, which is easy to build and quite accurate. At low frequencies, where the atmospheric opacities are low and the sky is very cold, receiver gain compression limits its accuracy.

4.2 Semitransparent 290 K vane

This is a variant of the chopper wheel method which minimizes the effects of gain compression. One attenuates the incoming sky signal, in effect terminating a fraction of the receiver beam at 290 K; extrapolates to obtain the response if a 290 K load filled the entire beam; then feeds the extrapolated response into the standard chopper wheel formalism. A key advantage is that the load filling factor (or vane attenuation) may be calibrated at any time on the telescope by observing an astronomical source; one does not rely on interpolating from a table generated in a faraway lab years before.

The vane technique has been used at BIMA to calibrate the receivers for observations of solar flares. One measures the receiver output on the Sun, with and without the vane in place. Then $P_{vane} - P_{sun}$ replaces $P_{load} - P_{sky}$ in the denominator of equation 5, while T_{sun} replaces T_{bg} in equation 6.

The vane can be a thin piece of absorber, or a beamsplitter or wire grid polarizer which reflects some fraction of the beam onto a room temperature load. For the BIMA system I first tried to use a thin sheet of antistatic polyethylene foam as an absorber, but nonuniformities in the foam and reflections from the surface spoiled the results. A dielectric beamsplitter mounted at an angle to the optical axis proved to be a better choice. Unfortunately the reflection coefficient of a beamsplitter is polarization sensitive, and the current BIMA system does not position the beamsplitter accurately enough to get good results.

4.3 290 K and 350 K loads

A warm load is much easier to make than a cold load. There is no problem with water condensation, so it can be insulated with styrofoam or other low-loss materials. The simulations show that a 350 K load is not particularly useful at 110 or 230 GHz because it is too different in temperature from the sky. It may be of value at higher frequencies, however, where receiver gain compression is less of a problem.

4.4 290 K and 80 K loads

This combination appears to have few benefits. The uncertainties introduced by gain compression are similar to those for the ordinary chopper wheel method.

4.5 80 K and 20 K loads

At 110 and 230 GHz, calibrating with 2 cold loads does greatly reduce the error from gain compression. Unfortunately, the uncertainty in the effective load temperatures (~ 1.2 K each, for loads differing by only 60 K), leads to a calibration uncertainty of order 3%.

Moving cold loads into the beams *inside* the dewar would work better, but requires moving parts in the dewar which are very undesirable.

4.6 300 K and 400 K loads in the subreflector

This technique has several outstanding advantages: (1) The loads are available for all receiver bands. (2) The calibration signal is small, so gain compression is not a problem. (3) Switching in the loads is unlikely to perturb any standing wave pattern between receiver and subreflector, so gain variations attributable to this pattern can be calibrated. (4) The loads contribute only 2–3 K DSB to the receiver noise temperature, so it is feasible to calibrate continuously to track variations in receiver gain or atmospheric opacity. The key disadvantage is that the coupling between the feed horn and the loads must be measured to better than 1 part in 10^4 ; this is an intimidating prospect. Another disadvantage is that the loads and the switching mechanism must be mounted in a relatively inaccessible location on the back of the subreflector.

5 Recommendations

- Provide high quality ambient and warm loads for each receiver. To get the lowest possible reflection coefficients it may be necessary to build several loads to handle different frequency ranges. The warm load(s) should be optimized for use at submm wavelengths.
- Do not bother with cold loads in the dewar. If the receiver beams must be directed back into these loads through vacuum windows, then reflection losses from the windows substantially degrade the calibration accuracy. Calibrating these window losses may be feasible in principle, but it is time-consuming and one will always have nagging doubts about the effective load temperatures.
- Provide a highly accurate τ -meter at the center of the array. This device may be as complicated as necessary. Monitoring the atmospheric temperature profile, perhaps with a 50 GHz radiometer, may be useful.
- Continue to develop the subreflector and semitransparent vane calibration techniques. These provide the best hope of correcting for receiver gain compression in the lower frequency bands.

6 References

Bock, D., Welch, J., Fleming, M., & Thornton, D. 1998, “Radiometric Calibration at the Cassegrain Secondary Mirror,” ALMA memo 225.

Engargiola, G., & Plambeck, R.L. 1998, “Wideband 3mm SIS mixers operated with partial saturation,” Proc. SPIE, 3357, pp. 508-518. (Also available as BIMA memo 65 at <http://bima.astro.umd.edu/memo>).

Feldman, M.J., Pan, S.-K., & Kerr, A.R. 1987, “Saturation of the SIS Mixer,” Extended Abstracts of the 1987 International Superconductivity Electronics Conference, pp. 290-292.

Holdaway, M.A., Radford, S.J.E., Owen, F.N., & Foster, S.M. 1995, “Data Processing for Site Test Interferometers,” ALMA memo 129.

Mangum, J., 2000, “Amplitude Calibration at Millimeter and Submillimeter Wavelengths,” ALMA memo 318.

Tucker, J.R., & Feldman, M.J. 1985, “Quantum Detection at Millimeter Wavelengths,” *Reviews of Modern Physics*, 57, 1055–1113.

Ulich, B.L., & Haas, R.W. 1976, “Absolute Calibration of Millimeter-Wavelength Spectral Lines,” *ApJS*, 30, 247.

Yun, M.S., Bastian, T., Holdaway, M., Mangum, J., & Welch, J., “Accurate Amplitude and Flux Calibration of the MMA,” ALMA memo 211.

Table 1. Fractional calibration errors at 110 GHz

variable	value	chop	vane	290/350	290/80	80/20	subr
τ	0.050 ± 0.002	.000	.000	.003	.003	.003	.003
T_m	260 ± 5	.002	.002	—	—	—	—
η	0.980 ± 0.005	.000	.001	.005	.005	.005	.005
G_s	0.500 ± 0.005	.010	.010	.010	.010	.010	.010
T_{load1}	290 ± 0.1	.000	.000	.002	.001	—	—
	80 ± 1.05	—	—	—	—	.018	—
	300 ± 0.11	—	—	—	—	—	.001
T_{load2}	350 ± 0.32	—	—	.005	—	—	—
	80 ± 1.05	—	—	—	.005	—	—
	20 ± 1.35	—	—	—	—	.022	—
	400 ± 0.56	—	—	—	—	—	.006
f	0.2 ± 0.0004	—	.002	—	—	—	—
	0.008 ± 0.00008	—	—	—	—	—	.010
T_{sat}	2500	.103	.020	.243	.126	.018	.002
TOTAL		.103	.023	.243	.127	.036	.016

Table 2. Fractional calibration errors at 230 GHz

variable	value	chop	vane	290/350	290/80	80/20	subr
τ	0.070 ± 0.0028	.000	.000	.004	.004	.004	.004
T_m	260 ± 5	.002	.002	—	—	—	—
η	0.980 ± 0.005	.001	.001	.005	.005	.005	.005
G_s	0.500 ± 0.005	.010	.010	.010	.010	.010	.010
T_{load1}	290 ± 0.1	.000	.000	.002	.001	—	—
	80 ± 1.05	—	—	—	—	.018	—
	300 ± 0.11	—	—	—	—	—	.001
T_{load2}	350 ± 0.32	—	—	.005	—	—	—
	80 ± 1.05	—	—	—	.005	—	—
	20 ± 1.35	—	—	—	—	.022	—
	400 ± 0.56	—	—	—	—	—	.006
f	0.2 ± 0.0004	—	.002	—	—	—	—
	0.008 ± 0.00008	—	—	—	—	—	.010
T_{sat}	10000	.025	.005	.057	.030	.003	.000
TOTAL		.027	.012	.059	.032	.031	.017

Table 3. Fractional calibration errors at 490 GHz

variable	value	chop	vane	290/350	290/80	80/20	subr
τ	1.1 ± 0.044	.027	.027	.068	.068	.068	.068
T_m	260 ± 5	.052	.052	—	—	—	—
η_l	0.980 ± 0.005	.001	.001	.005	.005	.005	.005
G_s	0.500 ± 0.005	.010	.010	.010	.010	.010	.010
T_{load1}	290 ± 0.1	.001	.001	.002	.000	—	—
	80 ± 1.05	—	—	—	—	.018	—
	300 ± 0.11	—	—	—	—	—	.001
T_{load2}	350 ± 0.32	—	—	.005	—	—	—
	80 ± 1.05	—	—	—	.005	—	—
	20 ± 1.35	—	—	—	—	.021	—
	400 ± 0.56	—	—	—	—	—	.006
f	0.2 ± 0.0004	—	.002	—	—	—	—
	0.008 ± 0.00008	—	—	—	—	—	.010
T_{sat}	50000	.001	.000	.004	.001	.006	.000
TOTAL		.059	.059	.069	.069	.075	.070

Appendix A. Definition of terms.

$K(T)$ is the receiver gain, in units of mW/Kelvin.

G_s and G_i are the normalized gains of the signal and image sidebands ($G_s + G_i = 1$).

η_l is the efficiency for rear spillover, blockage, and ohmic loss.

ν_s and ν_i are the signal and image frequencies; I assume $\nu_i = \nu_s - 16$ GHz.

τ_s and τ_i are the atmospheric opacities at zenith at the signal and image frequencies.

A is the airmass.

f is the fraction of the receiver beam filled by the load.

T_m is the effective physical temperature of the atmosphere.

T_{load} is the physical temperature of a load.

T_{spill} is the temperature at which spillover is terminated.

T_{bg} is the 2.7 K cosmic background temperature.

T_A is the antenna temperature of a source.